catalysts

MDPI

Article

Numerical Simulation and Experimental Study on Commercial Diesel Reforming Over an Advanced Pt/Rh Three-Way Catalyst

Hanyu Chen [1,*], Xi Wang [2,*], Zhixiang Pan [1] and Hongming Xu [3]

[1] School of Energy and Power Engineering, Wuhan University of Technology, Wuhan 430063, China
[2] School of Physical Education, Jianghan University, Wuhan 430056, China
[3] Department of Mechanical Engineering, University of Birmingham, Birmingham B15 2TT, UK
* Correspondence: chyu@whut.edu.cn (H.C.); wangxi050611024@126.com (X.W.)

Received: 11 June 2019; Accepted: 4 July 2019; Published: 7 July 2019

Abstract: Hydrocarbon fuel reforming has been proven useful for producing hydrogen that is utilized on road vehicles, but it is associated with reaction mechanism and catalyst characterization. In this study, a reduced mechanism for *n*-heptane/toluene reforming over an advanced Pt/Rh TWC is adopted to investigate the effects of the reaction conditions on H_2 and CO concentrations. The physical and chemical properties of the advanced catalyst are examined using SEM, XRD and XPS analyses. The contrasted experiments are conducted to study the composition variation tendency of the reforming reactor gas product. The results show that the POX reaction is most likely to occur considering the stoichiometric ratio of H_2/CO, and other reactions are SR or ATR. The coke formation and carbon deposition occur on the catalyst surface, and the diffraction peaks corresponding to the metallic Pt are observed, while no obvious peaks characteristic of Rh are detected. The characteristics of the concentration trend of *n*-heptane/toluene reforming can represent H_2 and CO yield features of diesel reforming in a way; nevertheless, the difference of the average H_2 and CO concentration is remarkable.

Keywords: diesel fuel reforming; *n*-heptane/toluene; hydrogen production; catalysts; simulation

1. Introduction

The potential risk of the use-up of fossil fuel has been looming over us, meanwhile, hydrogen fuel has long been proposed as a promising substitute to fossil fuel in both stationary and mobile devices in the near future [1]. The advantages of the fuel cell power generator on which hydrogen fuel derived from fossil fuel is utilize, mainly lie in enhancing the energy utilization efficiency and reducing poisonous gases emissions [2]. It is essential that an uninterrupted hydrogen supply for a fuel cell generation is set. Nevertheless, one of the biggest difficulties, particularly for mobile generation set, is the lack of existing infrastructure of hydrogen production nowadays [3]. In view of the foregoing case, some studies have sought to adopt hydrocarbon fuel reforming to supply hydrogen into fuel cell generation sets efficiently [4–11]. Compared to the traditional internal combustion engine generation sets, a diesel fuel cell auxiliary power unit (APU) possess the merits of higher energy utilization efficiency and lower harmful tailpipe emissions [6]. Increasing attention to the production of hydrogen is due to its conversion potential to clean liquid fuels free from sulfur such as diesel fuel; therefore there is great interest in converting diesel fuel into hydrogen. The techniques of how to convert diesel fuel into hydrogen that have been developed in the past are mainly partial oxidation reforming (POX), steam reforming (SR), autothermal reforming (ATR), or a combination of two or more of the above [5,12,13].

Due to the complexity of diesel fuel, its reforming process in hydrogen production is complicated, and different reactions can occur consecutively [14,15]. No single compound predominates in commercial diesel fuel, and some hypothetical compounds or surrogate fuels, such as *n*-heptane and toluene, that represent the key characteristics of diesel fuel, are critical and related research work is carried out in literature [16–20]. For example, *n*-heptane has been used as a single surrogate for diesel due to its similar ignitibility [16], while the drawbacks are also obvious as no other components are considered in those simplified approaches. Some studies also show that aromatics play a vital role in soot formation processes, and the aromatic content in diesel fuel is usually approximately 25–35% [17]. Therefore, more realistic multi-component surrogate models, taking the aromatic components into consideration, have been proposed for diesel fuel. Since the ignition delays of paraffin from C_7 to C_{16} are quite similar, it is possible to replace the *n*-decane component in diesel fuel surrogates with *n*-heptane, simpler paraffin to reduce the complexity of the surrogate model [17]. Therefore, the reference fuel (*n*-heptane and toluene) can be regarded as a foundation for the development of more realistic surrogate models. In the studies [18,19], the related research of the reference fuel (*n*-heptane and toluene) as surrogate diesel fuel mainly focuses on the chemical kinetic mechanism for combustion characteristics and the predictions of PAH species and soot emissions. Through the related research including ignition delay, laminar flame speed, and species profiles in flames, a reduced *n*-heptane/toluene mechanism can be deduced for diesel fuel in practical engine application. However, little research on the catalytic reforming mechanism of *n*-heptane/toluene as surrogate diesel fuel for hydrogen production has been conducted, and the published literature of diesel reforming mainly focuses on *n*-heptane as a diesel surrogate until now. For example, Abashar [20] studied the simultaneous hydrogen production of the catalytic reforming of *n*-heptane in CFFBR and CFFBMR. Hamoule et al. [21] investigated the catalytic activities of Pt catalysts coated on Al-HMS for *n*-heptane reforming. Gonzalez-Marcos et al. [22] investigated an industrial characterization method for naphtha reforming bimetallic Pt-Sn/Al_2O_3 catalysts by means of *n*-heptane reforming test reactions. Susu [23] studied the aromatization selectivity during *n*-heptane reforming on sintered Pt/Al_2O_3 and Pt-Re/Al_2O_3 catalysts. Does the *n*-heptane/toluene reforming represent the features of diesel fuel reforming in the typical reaction conditions? What is the differences of H_2 and CO concentration (Vol. %) between *n*-heptane/toluene reforming and diesel fuel reforming? Yet, the above questions remain unresolved.

In general, the reforming catalysts are composed of noble metals (Pt, Pd, Rh, etc.) supported on stabilized supports (Al_2O_3, CeO_2, ZrO_2, etc.) [24,25]. Among the different activity additives proposed in the published literature, CeO_2 remains outstanding due to its high oxygen storage capacity, oxidation/reduction reversibility of metals utilized as active phase, and offering assistance in carbon deposition elimination [26,27]. The advantages of Al_2O_3 are cheap, quite highly refractory, and relatively inert to water in a great variety of steam reforming conditions [28]. ZrO_2, ascribed to the crystal structure as fluorite, has the advantages of high thermal stability and protects the catalyst from being deactivated by carbon coking and sintering [29]. As reported in study [29], CeO_2 and ZrO_2 form $CeZrO_2$, which can impede the carbon coking or deposition of diesel fuel over the reforming catalyst. Achouri et al. [11] compared two different types of Ni-Al/Al_2O_3 catalysts which were prepared, respectively, by co-precipitation and wet impregnation techniques, by means of scanning electron microscopy (SEM), X-ray diffraction (XRD), and various temperature-programmed analyses before and after diesel steam reforming tests. In study [30], atomic layer deposition (ALD) was used to deposit Pt into KL zeolite channels, and Pt/KL catalysts showed excellent activity for the aromatization of *n*-heptane, high toluene selectivity, and prominent stability. Alvarez-Galvan et al. [31] evaluated the coke amount in aged catalysts by TG analysis, simultaneously the metal particle size was also calculated by TEM and XRD methods. A traditional three-way catalyst (TWC), installed widely in the tailpipe of the gasoline engine, usually is composed of platinum group metals dispersed on washcoated support materials [32,33]. In account of an outstanding ability of CeO_2-ZrO_2 solutions to store and release oxygen in compensating the deviations from ideal stoichiometric three-way running conditions, they are usually employed in TWC installed on the gasoline vehicles, in order to meet

the increasingly stringent emission regulations [34]. Therefore, the representative composition of TWC now is composed of noble metals or their alloys (as a rule Pt/Rh or Pd), CeO_2-ZrO_2 (usually $Ce_{0.5}Zr_{0.5}O_{2-\delta}$) and aluminum oxide, which ensures dispersion of two former components and also holds back the aggregation and deactivation of the catalyst [35]. The noble metals, such as Pt and Rh, are supported on stabilized supports, such as Al_2O_3, CeO_2 and ZrO_2, as the catalysts have been reported to facilitate the reforming of diesel fuel or light hydrocarbons in the abundant literature [24–31,36]. There are a few studies on the physical and chemical properties of TWC examined before and after diesel fuel reforming tests, and there are several aspects that need to be taken into account in diesel fuel reforming, many of which are associated with the catalytic material itself and the reforming process. In study [37], the catalytic activity of the water-gas shift and the steam reforming reactions over Pd/$Ce_{0.67}Zr_{0.33}O_2$-Al_2O_3 three-way catalysts was studied. In study [38], several catalysts for methane reforming in the absence of gaseous oxygen were discussed, and the conclusion that the doped ceria might open new catalytic routes for oxidation reactions without gaseous oxygen was determined. Nevalainen et al. [39] discussed the effects of exhaust gas composition and the ageing of TWC on the performances of catalysts. The above-mentioned scarce literature touched on the TWC reforming of methane and exhaust gas but did not refer to diesel fuel reforming over TWC. In addition, no studies on the physical and chemical characterization analysis of an advanced Pt/Rh TWC for diesel fuel reforming in the typical reaction conditions, have so far been reported in the literature.

The objective of diesel fuel reforming is to produce an amount of hydrogen, which is a supply for fuel cell generation sets. Granlund et al. [1] evaluated three bimetallic catalysts for autothermal reforming of diesel fuel, and H_2 yield as a function of time was discussed. In study [7], a highly dispersed 50 wt.% Ni/MgO-Al_2O_3 catalyst was prepared and pre-reforming reactions were carried out using *n*-tetradecane as a surrogate compound to diesel. In study [11], Ni-Al spinel catalysts were prepared, simultaneously H_2 and CO yield tests of diesel steam reforming were performed. Granlund et al. [40] compared a conventional monolith reactor for oxidative steam reforming of diesel fuel through 3 wt.% Rh supported on a high surface area of CeO_2-ZrO_2 and clarified H_2 yield and CO_2 selectivity. Mota et al. [41] studied catalysts derived from $LaCo_{1-x}Ru_xO_3$ perovskite precursors with high Ru loading in the oxidative reforming of diesel for hydrogen production. Grote et al. [42] described the optimization of a compact steam reforming based upon a catalytically coated micro heat exchanger for diesel fuel, and the dry reformate gas yield was analyzed. Wang and Huang et a.l [43,44] presented a new self-sustained electrochemical promotion catalyst and conducted a series of partial oxidation reforming tests on *n*-pentadecane and methane at temperatures of 450–650 °C, respectively. The above-mentioned studies mainly focused on H_2 and CO yield of diesel reforming or surrogate compounds of diesel reforming based on typical precious and non-precious metal catalysts. However, the simulation and compared tests on H_2 and CO concentration of surrogate diesel reforming, such as *n*-heptane/toluene, using an advanced Pt/Rh TWC in the typical reaction conditions have not been reported in the literature.

In our previous study [45], *n*-heptane was adopted as surrogate diesel fuel to simulate the diesel reforming over a Pt/CeO_2-Al_2O_3 catalyst of a diesel engine under medium load whose engine speed is 2000 r/min and load is 50% of the full load. Owing to the complexity of diesel fuel, a single compound as a surrogate diesel would still have certain defects on representing the characteristics of commercial diesel fuel. Therefore, further studies on multi-component fuel as surrogate diesel are needed to evaluate the features of diesel fuel reforming in the typical reaction conditions. In this paper, a reduced mechanism for *n*-heptane/toluene reforming over an advanced Pt/Rh TWC is adopted to investigate the effects of the reaction conditions on hydrogen production. The preferred reaction conditions (GHSV, O_2/C ratio, H_2O/C ratio, and reforming temperature) are determined, and these can guide the diesel reforming test in a laboratory reformer setup. In addition, the physical and chemical properties of an advanced Pt/Rh TWC are examined before and after diesel reforming tests, by several characterization techniques, including SEM, XRD, and XPS analyses. In the end, the comparison of reforming bench tests of diesel fuel and *n*-heptane/toluene in a laboratory mini reformer is conducted to study the

composition variation tendency of the reforming reactor gas product. The aim of this study is to bridge the gap of knowledge concerning the role of the numerical simulation of *n*-heptane/toluene as surrogate diesel fuel over advanced TWC for use in diesel reforming and to reveal the changing trend of H_2 and CO concentrations between diesel fuel reforming and *n*-heptane/toluene reforming.

2. Theory and Experiment

2.1. Catalytic Reforming Kinetics of Representative Hydrocarbons

In this study, the basic reactions are endothermic steam reforming (SR) (Equation (1)), exothermic partial oxidation (POX) (Equation (2)), autothermal reforming (ATR) (Equation (3)) as a combination of SR and POX, as well as water-gas shift reaction (Equation (4)) in a self-designed mini reformer. The *n*-heptane/toluene reforming process can be modeled by the following reaction steps:

$$C_nH_m + nH_2O \rightarrow (m/2 + n)H_2 + nCO\,\Delta H > 0 \quad (1)$$

$$C_nH_m + (n/2)O_2 \rightarrow (m/2)H_2 + nCO\,\Delta H < 0 \quad (2)$$

$$C_nH_m + (n/2)H_2O + (n/4)O_2 \rightarrow (m/2 + n/2)H_2 + nCO\,\Delta H \leq 0 \quad (3)$$

$$CO + H_2O \leftrightarrow H_2 + CO_2\,\Delta H = -41 kJ/mol \quad (4)$$

As illustrated in the literature [42], the corresponding rate equation which is used in this study for Equation (1) is given by:

$$r_1 = k_1 C_{C_nH_m}^{a} C_{H_2}^{-b} \quad (5)$$

$$k_1 = k_0 \exp\left[\frac{-E_a}{R}\left(\frac{1}{T} - \frac{1}{T_0}\right)\right] \quad (6)$$

where r_1 is the reaction rate, k_0 and k_1 are the rate constants of the reforming reaction, C is the molar yield of species, a and b are the exponents of reaction rates, E_a is the activation energy, and T is the reaction temperature. Note that the reaction rate constant k_0 is adjusted in response to the activity of the catalysts coating.

Assuming that the CO shift reaction is not limited by the kinetic effects, an equilibrium reaction rate can be used for reaction Equation (4):

$$r_2 = k_f C_{CO} C_{H_2O} - k_b C_{H_2} C_{CO_2} \quad (7)$$

$$k_b = \frac{k_f}{K_p} \quad (8)$$

$$K_P = 4290{\cdot}1 \exp\left(\left(\frac{1K}{T} - 0.001\right) 1.4664\right) \quad (9)$$

where r_2 is the reaction rate, k_f is the rate constant of the forward shift reaction, C is the molar yield of species, k_b is the rate constant of the backward shift reaction, T is the reaction temperature, K_P is the equilibrium constant of the shift reaction and fitted in the selected temperature range.

Simultaneously the corresponding rate equation, as illustrated in study [44], which is used in this study for Equation (2) is given by:

$$r_0 = k \frac{K_{C_nH_m} P_{C_nH_m} K_{O_2} P_{O_2}}{\left(1 + K_{C_nH_m} P_{C_nH_m} + K_{O_2} P_{O_2}\right)^2} \quad (10)$$

$$k = A \exp\left(\frac{-E}{RT}\right) \quad (11)$$

where r_0 is the reaction rate, k is the reaction rate constant which is written in Arrhenius-type expression, $P_{C_nH_m}$ and P_{O_2} are the partial pressure of the reactants, A is the pre-exponential factor, E is the activation energy, R is the gas constant, T is the reaction temperature, $K_{C_nH_m}$ and K_{O_2} are the adsorption constants for C_nH_m and O_2, respectively.

In general, the catalytic reforming mechanisms of representative hydrocarbons merge the gas phase chemical kinetics into surface reaction chemical kinetics. In this study, a reduced mechanism for *n*-heptane/toluene reforming with 71 species and 360 reactions, which stems from the Lawrence Livermore National Laboratory (LLNL) and related literature, is proposed [46]. Propene is one of the major pollutants and usually is regarded as a representative of unburnt hydrocarbons [45,47,48], and the surface reaction mechanism of propene can be adopted to evaluate the performance of platinum/rhodium catalyst. The gas-phase chemical kinetics of *n*-heptane/toluene and the surface reaction chemical kinetics are illustrated in studies [45,46]. The interactive reactions between *n*-heptane and toluene are listed in Table 1. In Table 1, A is the pre-exponential factor, n is temperature index, and E is the activation energy.

Table 1. Rate constant expressions and interactive reactions between *n*-heptane and toluene.

Reaction Step	Elementary-Step Reaction	A	n	E
R.208	$C_7H_{15-2} + C_7H_8 = C_7H_7 + nC_7h_{16}$	1.00×10^{11}	0.0	12,000.0
R.209	$A_{1-} + nC_7H_{16} = C_7H_{15-2} + A_1$	2.00×10^{11}	0.0	12,500.0

With regard to the prototype diesel engine operating conditions [49], the Gas Hourly Space Velocity (GHSV; volumetric flow rate of gas per hour divided by the volume of the catalyst bed) is set to 10,000, 15,000, 20,000, and 25,000 1/h. The O_2/C molar ratio is set to 0.3, 0.4, 0.5, and 0.6. The H_2O/C molar ratio is set to 0.5, 1.0, 1.5, and 2.0. The reaction temperature is set to 425, 465, 505, and 545 °C. Gas-phase reactions and surface reactions are modeled by an elementary-step reaction mechanism based on the molecular processes, meanwhile, the surface reaction mechanisms of propene are applied to investigate the reforming products over the Pt/Rh catalysts. The models described in the previous chapters are implemented in the commercial Chemkin code [50], and the chemical kinetics files are available in Chemkin format in this study. The reactions are considered by implementing specific sources at the advanced TWC catalyst surface. The *n*-heptane/toluene (mole ratio: 3.0/1.0) as surrogate diesel fuel is applied to all computations presenting diesel fuel. The schematic diagram of *n*-heptane/toluene reforming over Pt/Rh catalysts carried out in Chemkin is shown in Figure 1. In Figure 1, reactants are set in the Inlet source module, reaction properties and the mechanisms of gas-phase reactions, and surface reactions are carried out in the Reforming reactor module, and the reaction products of H_2 and CO are monitored in the Reforming product module.

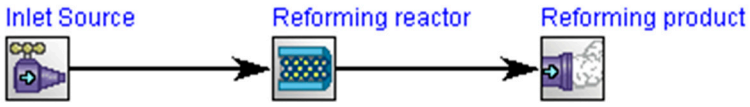

Figure 1. Schematic of *n*-heptane/toluene reforming in Chemkin.

2.2. Catalyst Preparation

The three-way catalyst usually consists of a ceramic substrate, a support layer, and an active layer of noble metals. In this study, a bimetallic catalyst is first impregnated on alumina, and then this is applied on the monolith, in which Pt/Rh content is approximately 2.0 wt%, and the weight ratio of $Ce_{0.5}Zr_{0.5}O_{2-\delta}/Al_2O_3$ is 2.0/5.0. To prepare the catalyst, the alumina powder is impregnated with the metals by the incipient wetness technique, simultaneously the impregnated powders are mixed with an appropriate quantity of distilled water to obtain slurries. This preparation procedure is repeated twice with a drying step at 110 °C for 3 h in between. The capillary forces of the selected slurries on

the monolith are intensively monitored and controlled by pulsing air using a blow dryer. After that, the coated monoliths are calcined at 800 °C for 3 h to obtain the fresh catalysts.

2.3. Catalyst Characterizations

The TWC catalyst powder samples (before and after the diesel reforming tests) in this study are characterized by the following techniques:

- Scanning Electronic Microscopy (SEM) is adopted using a JSM-5610LV (JEOL Ltd., Tokyo, Japan) and energy-dispersive X-ray spectroscopy (EDXS) with a Phoenix detector (EDAX, Mahwah, NJ, USA). The fresh catalyst samples are deposited on carbon double-face tape for SEM and EDXS analysis, simultaneously they are substituted with silicon supports for used catalysts to analyze the carbon deposition.
- X-ray diffraction (XRD) is adopted to determine the crystal phase of the powder samples. A Bruker D8 Advance scanning 2θ from 10° to 90° in the scan mode (0.02°, 1s), using Ni filtered Cu Kα radiation is employed. The samples are pre-reduced offline under an H_2 flow at 500 °C for 2 h. The crystal phase is identified by comparing the diffractograms with powder diffraction files.
- X-ray photoelectron spectroscopy (XPS) is conducted using a Thermo Fisher Scientific ESCALAB 250xi scanning ESCA microprobe (Waltham, MA, USA) with double anode Al/Mg radiation and a multichannel detector. Prior to the measurement, the samples are reduced in H_2 at 400 °C for 2 h.

2.4. Experimental Procedure

In this study, the reforming tests of H_2 and CO concentration (Vol. %) are conducted in a self-designed mini reformer. The catalytic reformer setup, as shown in Figure 2, is mainly composed of carrier gas supply (Ar), water, oxygen, diesel fuel, *n*-heptane/toluene supply, advanced TWC, furnace temperature controller, and reforming reactor product gas analyzer. The catalytic reforming reactor is fed by water, oxygen, diesel fuel, or *n*-heptane/toluene, and it is loaded with an advanced Pt/Rh TWC. The reactor is placed in a tubular furnace, and the temperature is controlled by means of a temperature controller. In addition, a micro-evaporator is placed in the inlet of the reactor aimed to make sure water, diesel fuel, or *n*-heptane/toluene evaporating. A K-type thermocouple is adopted, and its layout is allowed vertical movement of the mixture, and thus, supervising the reactor temperature profile. Two syringe pumps fitted with a glass syringe are selected to supply water, diesel fuel, or *n*-heptane/toluene, as well as to control their flow rate, respectively. A gas chromatograph-mass spectrometer (GC-MS) model Agilent 7890B / 5977B MSD is used to measure the reactor products content, such as H_2 and CO. Before the content test of the reactor products, the GC-MS device ought to be calibrated with gas compositions of H_2 and CO close to the range the measurements. Note that the averaged test results in six replicates are used for all experiments and their standard deviations are less than 5%.

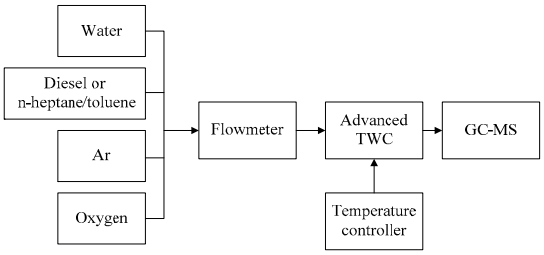

Figure 2. Schematic of reforming experimental setup.

3. Results and Discussion

In the previous literature [1,7,11,40–44], hydrogen or carbon monoxide yield of fuel reforming is defined as follows:

$$H_2 \text{ (or: CO) yield (\%)} = \text{mole amount of } H_2 \text{ (or: CO) in reformate/maximum theoretical mole amount of } H_2 \text{ (or: CO)} \times 100 \quad (12)$$

It is vital that the amounts of hydrogen account for the total reforming products in the practical fuel cell application. Therefore, hydrogen or carbon monoxide concentration of fuel reforming is proposed and defined in this study as follows:

$$H_2 \text{ (or: CO) concentration (\%)} = \text{mole amount of } H_2 \text{ (or: CO) in reformate/total mole amount of reforming products} \times 100 \quad (13)$$

3.1. Effect of Reaction Temperature on Reformer Product

Figure 3 shows the simulation results of the H_2 and CO concentration (Vol. %) for *n*-heptane/toluene reforming at the different reaction temperatures. The variation trends of H_2 and CO concentrations (Vol. %) are similar to the increased catalyst length. The maximum H_2 and CO concentrations escalate until a plateau (8.9% H_2 and 13.4% CO) while ensuring adequate catalyst length, as illustrated in Figure 3. Through the comparison of H_2 and CO concentration, the preferred reaction temperature is near to 505 °C. In consideration of the stoichiometric ratio of H_2/CO, the POX reaction is most likely to occur during the reaction process due to the partial oxidation reforming of toluene as discussed in the literature [4,25,31], and other reactions involved in *n*-heptane/toluene reforming may be SR or ATR.

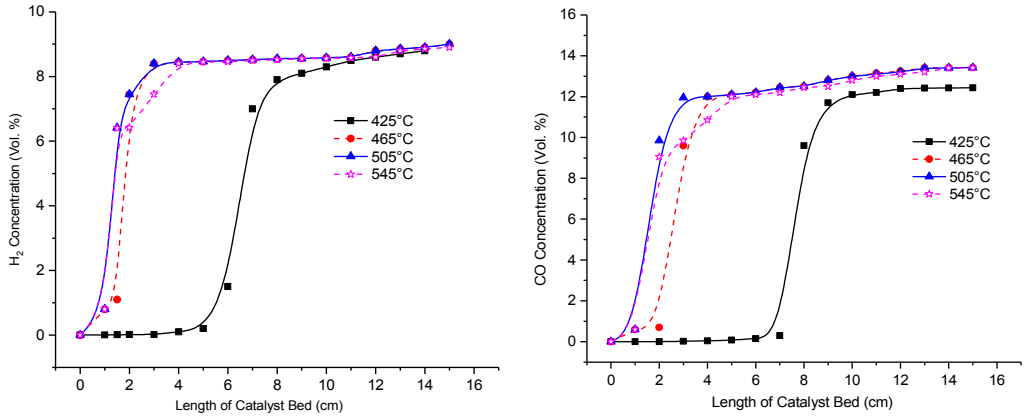

(**a**) H_2 (**b**) CO

Figure 3. Reaction temperature effect on H_2 and CO concentration.

3.2. Effect of GHSV on the Reformer Product

As is observed in Figure 4, the simulation results of H_2 and CO concentration (Vol. %) move toward unity as the decreased GHSV. Higher GHSV shortens the residence time of the reforming mixture within the catalyst, so the better catalytic activity of Pt/Rh TWC is required. The maximum H_2 and CO concentration (Vol. %) exceed 8.9% and 11.9%, and are kept constant while ensuring the adequate catalyst length, separately, as shown in Figure 4. The peak concentration velocity of H_2 and CO appear at the front part of the catalyst bed, the same findings are illustrated in the literature [14,51], and then it decreases as the increased axial length of the catalyst bed. Through the comparison of the H_2 and CO concentration, the preferred GHSV is 10,000 1/h.

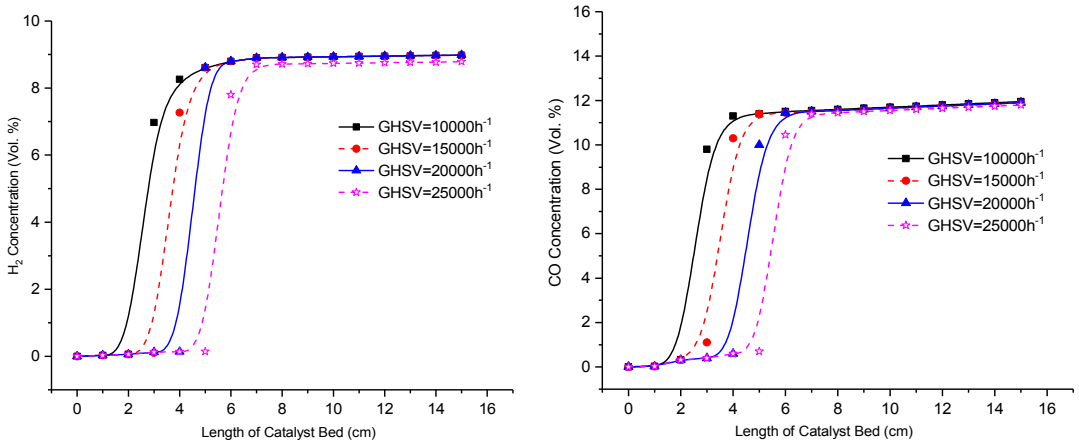

(**a**) H2 (**b**) CO

Figure 4. GHSV effect on H_2 and CO concentration.

3.3. Effect of H_2O/C Ratio on Reformer Product

As shown in Figure 5, the concentration (Vol. %) of H_2 and CO for *n*-heptane/toluene reforming surge as the increased H_2O/C ratio, and the corresponding maximum concentration (Vol. %) reach 9.3% and 11.6%, respectively. Higher H_2O/C ratio indicates the water is added in the reforming reactor. Compared to the results in Figures 3 and 4, the new reaction in Figure 5 occurring with water addition is probably WGSR, and it is demonstrated with the decreased CO concentration. The further increase of water addition significantly enhances hydrogen concentration by the WGSR as illustrated in the literature [52]. It can be concluded that the optimization of the reforming reaction condition and the catalyst to obtain the further conversion of the carbon monoxide to hydrogen by the WGSR will boost the produced hydrogen levels even further. Through the comparison of H_2 and CO concentration, the preferred H_2O/C ratio is 2.0.

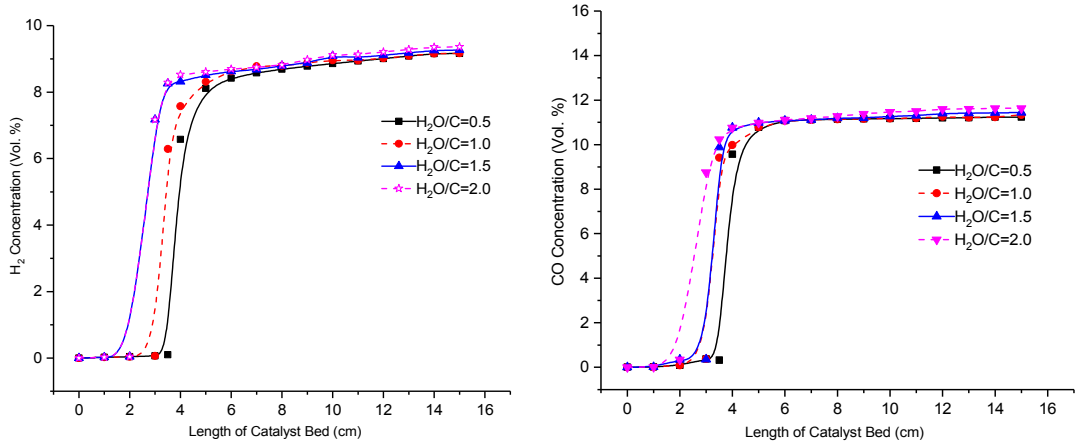

(**a**) H2 (**b**) CO

Figure 5. H_2O/C ratio effect on H_2 and CO concentration.

3.4. Effect of the O_2/C Ratio on Reformer Product

For the different GHSV and fuel flow rates into the catalyst bed, the corresponding O_2/C ratios are 0.3, 0.4, 0.5, and 0.6, separately. Figure 6 indicates the simulation results of H_2 and CO concentration (Vol. %) for *n*-heptane/toluene reforming at the different O_2/C ratio conditions. The concentration (Vol. %) of H_2 and CO are enhanced significantly with the increased O_2/C ratio, and the corresponding maximum concentration (Vol. %) reaches 18.4% and 17.2%, respectively. An increase in the O_2/C ratio means an increase in the quantity of oxygen reacting with hydrogen and carbon monoxide. The related result is also confirmed that the O_2/C ratio of the reactants has a strong influence on the H_2 and CO concentrations owing to the POX of hydrocarbons as illustrated in the literature [53,54]. Considering the stoichiometric ratio of H_2/CO, the POX and ATR reactions are most likely to occur in the reaction process. Through the comparison of the H_2 and CO concentration, the preferred O_2/C ratio is 0.6.

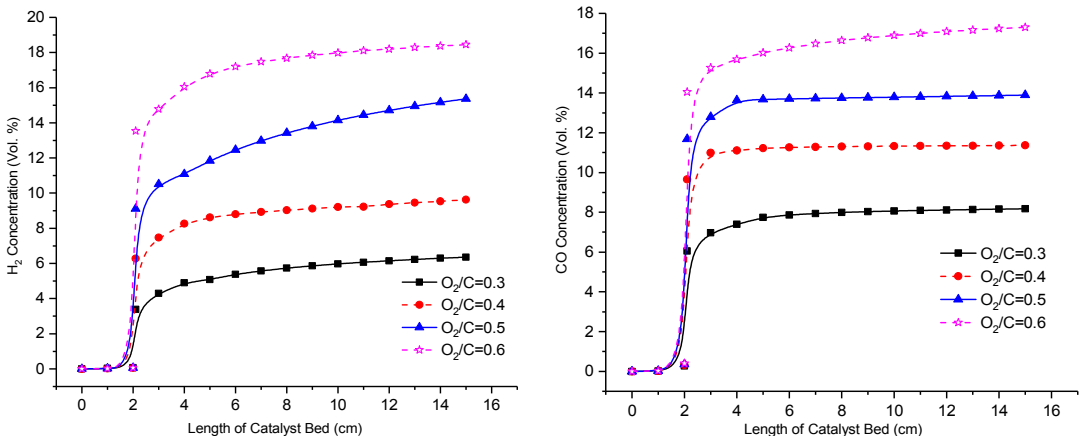

(**a**) H_2 (**b**) CO

Figure 6. O_2/C ratio effect on H_2 and CO concentration.

3.5. Sensitivity and Rate-of-Production Analysis of the H_2 Concentration

Figures 7 and 8 show the sensitivity and rate-of-production (ROP) analysis of the H_2 production for *n*-heptane/toluene reforming in the preferred reaction conditions (reaction temperature 505 °C, GHSV 10000 1/h, H_2O/C ratio 2.0, and O_2/C ratio 0.6), respectively. Sensitive analyses is adopted to investigate the dependence of the important reactions on the concentration of H_2. A positive sensitivity shows an increase in H_2 concentration and conversely a negative value indicates a decrease in the H_2 concentration. It is seen from Figure 7, that the reaction of OH/H_2O_2 chemistry and the H abstraction reaction of *n*-heptane by OH are the most sensitive reactions on the H_2 concentration. The ROP analysis can identify the contribution degree of the reaction steps on the H_2 concentration. Figure 8 shows that the reactions (R_{39}, R_{53}, R_{72}, and R_{77}) have significant effects on the H_2 concentration and the ROP coefficient occurs in jumping at the axial length of 2.32 cm for the catalyst bed. The total ROP coefficient is positive which illustrates that the reforming process of *n*-heptane/toluene moves forward with the H_2 concentration, although the ROP coefficient of R_{39} presents a negative value at a certain length of the catalyst bed.

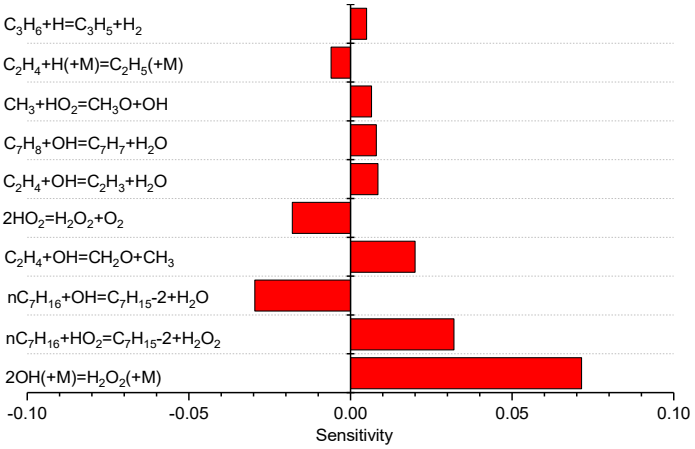

Figure 7. Sensitivity analysis of H_2 concentration in the preferred reaction conditions.

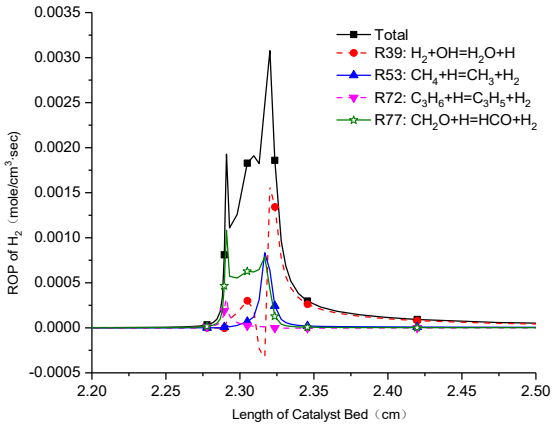

Figure 8. ROP analysis of H_2 concentration in the preferred reaction conditions.

3.6. Texture Analysis of the Catalyst

The Pt/Rh TWC performance is tested using a self-designed mini reformer with 2.0 g of catalyst powder samples dispersed in a 6 cm quartz wool bed and then placed in the middle of a 48 cm reactor length. The total flow rate is kept constant at 300 cm^3/min, which corresponds to a GHSV condition of 10000 1/h. A feed mixture of diesel and water emulsion with H_2O/C = 2.0 molar ratio is vaporized in the inlet of the micro-evaporator at 380 °C, before entering the diesel reforming reaction zone. The reactants, including diesel, water and oxygen, are pushed by argon as a carrier gas ensuring O_2/C = 0.6 molar ratio. The catalyst powder samples (before and after diesel reforming tests) are analyzed by SEM/EDXS, XRD, and XPS analyses.

The morphology of the advanced Pt/Rh TWC is investigated by SEM/EDXS analysis. Figure 9 shows SEM images of the fresh and used catalysts with the EDXS results. The fresh catalyst in Figure 9a exhibits a homogeneous surface with uniformity in the particle distribution; nevertheless, the used catalyst in Figure 9c reveals detail of agglomeration and heterogeneity in the morphology as discussed in the literature [25]. The average composition analysis by EDXS for the fresh and used catalysts is shown in Table 2. Figure 9 and Table 2 also show that the coke formation and carbon deposition take place on the TWC catalyst surface and similar observations have also been reported in previous studies [5,36], although $CeZrO_2$ is supposed to impede carbon deposition on the catalyst active site ascribed to its high lattice oxygen mobility [29].

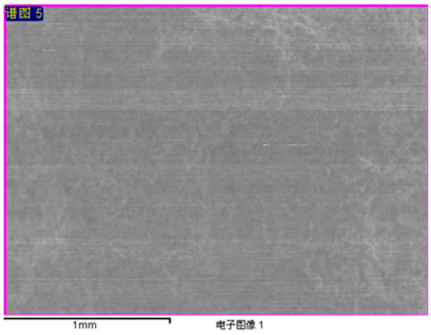

(**a**) SEM image (fresh)

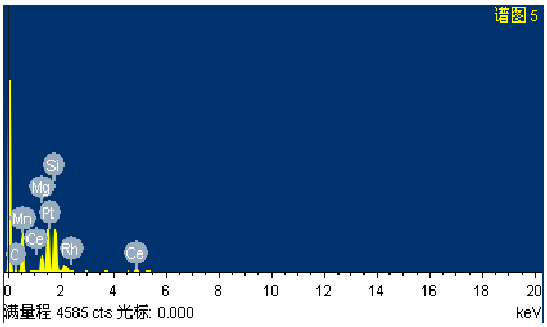

(**b**) Component analysis by EDXS (fresh)

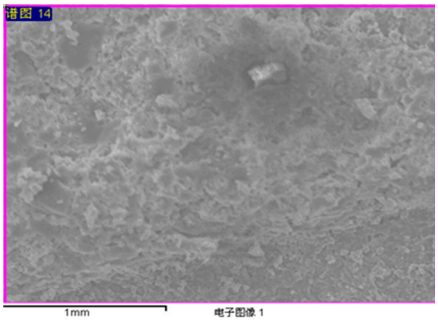

(**c**) SEM image (used)

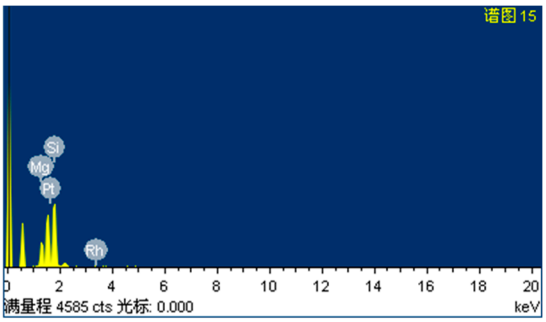

(**d**) Component analysis by EDXS (used)

Figure 9. SEM/EDXS analysis of an advanced TWC sample (fresh and used catalysts).

Table 2. Quantitative analysis of the composition measured by EDXS.

Catalysts	Average Composition (wt %)								
	C	O	Mn	Al	Si	Pt	Rh	Ce	Zr
Fresh	1.99	47.5	1.03	15.66	23.02	1.12	0.08	4.83	4.77
Used	8.09	40.35	1.18	13.52	25.39	2.05	0.06	4.29	5.07

Figure 10 illustrates the XRD patterns of the Pt/Rh TWC catalysts in the fresh state and after the used state. As shown in Figure 10, diffraction peaks ascribed to metallic Pt are observed at 2θ = 34, 46.5 and 81.5°, similar to findings in the literature [36]. In general, platinum oxide, e.g., PtO, is unstable and can easily decompose and form metallic Pt at the temperature over 500 °C [36]. In addition, no obvious peaks characteristic of Rh are detected, which can be ascribed to the low content of Rh and implies that Rh species are in a highly dispersed state. A diffraction peak at 2θ = 28.6°, shown in Figure 10, indicates the metallic Ce is observed, as discussed in the literature [5]. The formation of a porous CeO_2 phase is conducive to boost the specific surface area of the Ce-Zr support.

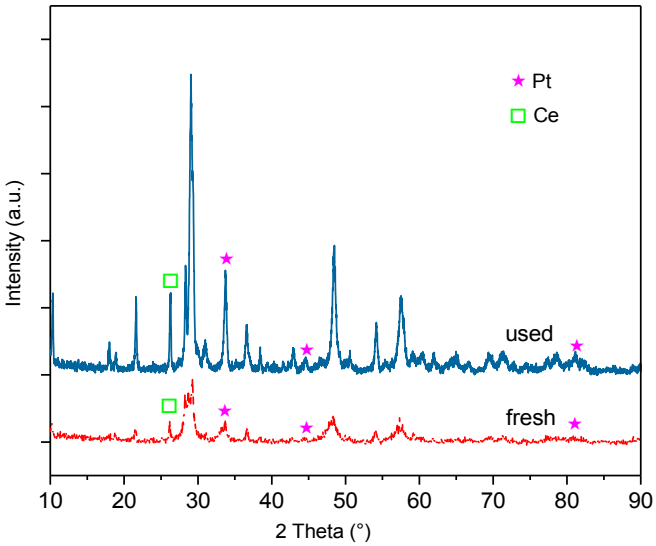

Figure 10. XRD patterns of Pt/Rh TWC catalysts for 2θ between 10° and 90° in the fresh state and after the used state.

The surface analysis of the catalysts (fresh and used catalysts) is performed by X-ray photoelectron spectroscopy (XPS). The XPS results in the expected detection of Pt, Rh, O, Ce, C, and Zr on the surfaces of the catalysts studied. Table 3 summarizes the results derived from the quantitative analysis of the XPS data. The quantitative surface analysis of the catalysts is based on the following peaks: Pt4f (74.1 eV), Rh3d (306.1 eV), O1s (531.1 eV), Ce3d (897.8 eV), C1s (284.2 eV), and Zr3d (182.9 eV). As seen in Table 3, most elements are found in the oxidized state. Rh is found to be present in its oxidized state, possibly in the form of Rh_2O_3, as illustrated in the literature [55]. Due to the binding energy overlap with Al peaks, the Pt4f peak is examined although only small traces of Pt are detected on the surface. For ceria, the binding energy of the Ce3d line is found at approximately 897.8 eV, indicating CeO_2 [55]. Hence, CeO_2 species are present on the surface of the catalysts as previously discussed by EDXS analysis. The C1s peak, a C–C bond peak or adventitious carbon peak, indicates the presence of a C=O or carbonate species. Therefore, this indicates that carbon deposition is taking place on the surface of the used catalyst. It is also clearly observed in Table 3 that there is an increase of the carbon surface concentration in the used catalysts, whereas an opposite trend resulted for Pt and Rh showing a decrease in the surface concentration.

Table 3. Quantitative surface analysis of the Pt/Rh TWC catalysts based on XPS results.

Catalysts	Average Surface Composition (atoms %)					
	Pt	Rh	O	Ce	C	Zr
Fresh	0.74	0.32	65.46	3.28	21.87	3.23
Used	0.41	0.2	33.88	1.43	51.9	7.45

Figure 11 shows the Pt4f and C1s spectra of the fresh and used Pt/Rh TWC catalysts. From the XPS profiles in Figure 11, it can be seen that the Pt4f and C1s peaks of the used Pt/Rh TWC catalyst shift to a lower binding energy compared to that of the fresh catalyst due to the interaction between the Pt (or C) species and the electron-donor sites in the Ce-Zr support, as discussed in the literature [25,30]. This result is in agreement with data derived from Table 3 in which the carbon surface concentration shows an increase while the Pt and Rh surface concentration reveals a decrease.

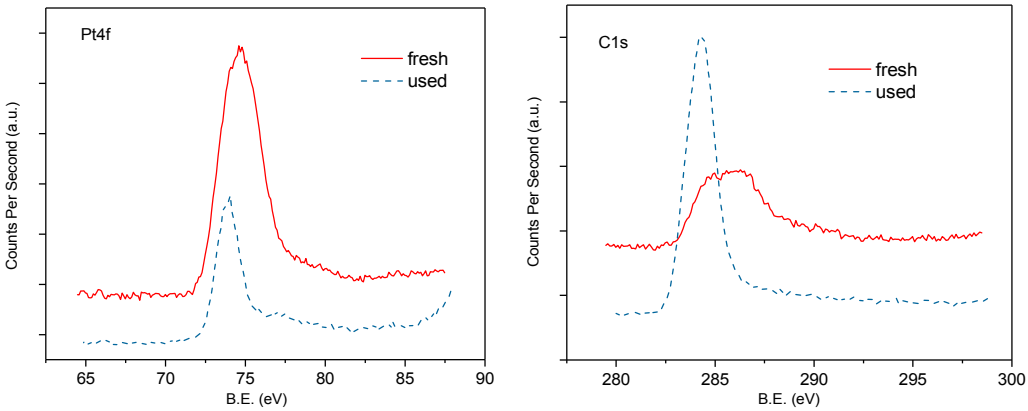

(**a**) Pt4f (**b**) C1s

Figure 11. XPS patterns of Pt4f and C1s photoemission spectra of the of Pt/Rh TWC catalysts.

3.7. Experimental Analysis Results of H_2 and CO Production

The sampling points of concentration are taken at the different catalyst length, and the averaged test results in six replicates are drawn. Figure 12 illustrates the experimental contrast results and error bars of the analysis of the H_2 and CO concentration (Vol. %) in the preferred reaction conditions described in Section 3.6. As shown in Figure 12, the average H_2 and CO concentration (Vol. %) of the diesel reforming experiment over the Pt/Rh TWC catalyst in the outlet of the reactor is 9.1% and 7.6%, respectively. Meanwhile, the average H_2 and CO concentration (Vol. %) of the *n*-heptane/toluene reforming experiment is 18.1% and 16.7%, respectively. The standard deviation of the average outlet of the H_2 concentration (Vol. %) for the diesel and *n*-heptane/toluene reforming experiment is less than 0.82% and 0.9%, respectively; the corresponding standard deviation of the average CO concentration (Vol. %) for diesel and *n*-heptane/toluene experiment is less than 0.7% and 0.75%. The average outlet H_2 and CO concentration (Vol. %) for diesel experiment compared to *n*-heptane/toluene experiment reduces by 49.8% and 54.5%, respectively.

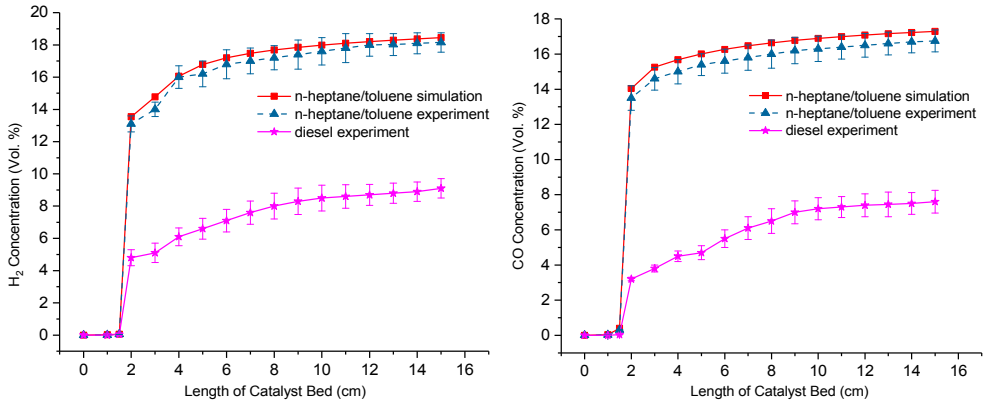

(**a**) H_2 (**b**) CO

Figure 12. H_2 and CO concentration comparison and Error bars analysis.

Through the comparison of reforming bench tests of diesel and *n*-heptane/toluene, the change trend of H_2 and CO concentration (Vol. %) reveals consistence as shown in Figure 12 while the difference of the average H_2 and CO concentration (Vol. %) results is remarkable. The reduction amount of H_2 and CO concentration (Vol. %) for diesel reforming compared to *n*-heptane/toluene reforming, maintained approximately 50% and 55%, is achieved over Pt/Rh TWC catalyst in the preferred reaction

conditions, respectively. The characteristics of concentration (Vol. %) trend for *n*-heptane/toluene reforming can represent the H_2 and CO yield features for diesel reforming in a way. The primary cause in aforementioned phenomenon is attributed to different components in commercial diesel fuel with different classes of chemical structures that are affected by different reaction conditions during the reforming process. In order to benefit from representing the diesel reforming as accurately as possible by means of numerical simulation method, a multi-component wide distillation surrogate fuel ought to be proposed in further studies [17].

As shown in the literature [1,7,11,40–44], the conversion and hydrogen and carbon monoxide yield were compared and analyzed which accounted for catalytic activity, operation time, reaction temperature, and other reaction conditions. However, the hydrogen and carbon monoxide concentration in the reforming products of diesel reforming over advanced Pt/Rh TWC catalyst is analyzed in this study concerning the practical on-board hydrogen production application. The characteristics of hydrogen concentration (Vol. %) trend in the reforming products in this study approximately coincide with those in the literature [14,51,52].

4. Conclusions

The results presented in this study provide a deeper understanding regarding the possible reaction mechanisms occurring on the H_2 and CO yield during *n*-heptane/toluene reforming over the Pt/Rh TWC catalyst that is analyzed by SEM/EDXS, XRD, and XPS analyses. The following are conclusions drawn from the results and discussion.

- In consideration of the stoichiometric ratio of H_2/CO, the POX reaction is most likely to occur during the reaction process owing to the partial oxidation reforming of toluene, and other reactions involved in *n*-heptane/toluene reforming may be SR or ATR.
- The optimization of the reforming reaction conditions and the catalyst to acquire further conversion of the carbon monoxide to hydrogen by the WGSR will boost the produced hydrogen levels even further. The preferred reaction conditions (reaction temperature 505 °C, GHSV 10000 1/h, H_2O/C ratio 2.0 and O_2/C ratio 0.6) are determined.
- The reaction of OH/H_2O_2 chemistry and the H abstraction reaction of *n*-heptane by OH are the most sensitive reactions on the H_2 yield, as well as the reforming process of *n*-heptane/toluene moves forward to H_2 yield.
- The coke formation and carbon deposition take place on the catalyst surface by SEM/EDXS and XPS analysis. The diffraction peaks ascribed to metallic Pt are observed, and no obvious peaks characteristic of Rh are detected by the XRD pattern analysis.
- The characteristics of concentration trend for *n*-heptane/toluene reforming can represent the H_2 and CO yield features for diesel reforming in a way, while the difference of the average H_2 and CO concentration results is remarkable. In order to benefit from representing the diesel reforming as accurately as possible by means of a numerical simulation method, a multi-component wide distillation surrogate fuel ought to be proposed in further studies.
- Future work comprises the investigation of the different impacts of a multi-component wide distillation surrogate fuel reforming on the H_2 and CO concentration. Additionally, the plan is to study the physical and chemical properties of the catalyst before and after surrogate diesel reforming tests.

Author Contributions: H.C. conceived and developed the paper; X.W. conducted the simulation and experiments; Z.P. and H.X. provided guidance and reviews throughout the development of this paper.

Funding: This research was funded by "State Key Laboratory of Engines at Tianjin University (K2018-09)", "the Key Laboratory of Marine Power Engineering & Technology, Ministry of Transport (KLMPET 2016-01)" and "research fund of Center for Materials Research and Analysis, WHUT (2018KFJJ07)".

Acknowledgments: The authors would like to thank CSSC Huangpu Wenchong Shipbuilding Company Limited for financial support.

Conflicts of Interest: The authors declare no conflict of interest.

Nomenclature

TWC	three-way catalyst
SEM	scanning electron microscopy
XRD	X-ray diffraction
XPS	X-ray photoelectron spectroscopy
POX	partial oxidation reforming
SR	steam reforming
ATR	autothermal reforming
PAH	polynuclear aromatic hydrocarbons
CFFBR	circulating fast fluidized bed reactors
CFFBMR	circulating fast fluidized bed membrane reactors
ALD	atomic layer deposition
TG	thermal gravimetric
GHSV	gas hourly space velocity
WGSR	water-gas shift reaction
ROP	rate-of-production
EDXS	energy-dispersive X-ray spectroscopy

References

1. Granlund, M.Z.; Jansson, K.; Nilsson, M.; Dawody, J.; Pettersson, L.J. Evaluation of Co, La, and Mn promoted Rh catalysts for autothermal reforming of commercial diesel: Aging and characterization. *Appl. Catal. B Environ.* **2015**, *172*, 145–153. [CrossRef]
2. Xu, X.; Li, P.; Shen, Y. Small-scale reforming of diesel and jet fuels to make hydrogen and syngas for fuel cells: A review. *Appl. Energy* **2013**, *108*, 202–217. [CrossRef]
3. Bowers, B.; Zhao, J.; Ruffo, M.; Khan, R.; Dattatraya, D.; Dushman, N.; Beziat, J.; Boudjemaa, F. Onboard fuel processor for PEM fuel cell vehicles. *Int. J. Hydrogen Energy* **2007**, *32*, 1437–1442. [CrossRef]
4. Han, G.; Lee, S.; Bae, J. Diesel autothermal reforming with hydrogen peroxide for low-oxygen environments. *Appl. Energy* **2015**, *156*, 99–106. [CrossRef]
5. Tribalis, A.; Panagiotou, G.D.; Bourikas, K.; Sygellou, L.; Kennou, S.; Ladas, S.; Lycourghiotis, A.; Kordulis, C. Ni Catalysts Supported on Modified Alumina for Diesel Steam Reforming. *Catalysts* **2016**, *6*, 11. [CrossRef]
6. Dolanc, G.; Pregelj, B.; Petrovčič, J.; Pasel, J.; Kolb, G. Control of autothermal reforming reactor of diesel fuel. *J. Power Sources* **2016**, *313*, 223–232. [CrossRef]
7. Koo, K.Y.; Park, M.G.; Jung, U.H.; Kim, S.H.; Yoon, W.L. Diesel pre-reforming over highly dispersed nano-sized Ni catalysts supported on MgO–Al2O3 mixed oxides. *Int. J. Hydrogen Energy* **2014**, *39*, 10941–10950. [CrossRef]
8. Zhou, W.; Ke, Y.; Wang, Q.; Wan, S.; Lin, J.; Zhang, J.; Hui, K. Development of cylindrical laminated methanol steam reforming microreactor with cascading metal foams as catalyst support. *Fuel* **2017**, *191*, 46–53. [CrossRef]
9. Martin, S.; Kraaij, G.; Ascher, T.; Baltzopoulou, P.; Karagiannakis, G.; Wails, D.; Wörner, A. Direct steam reforming of diesel and diesel–biodiesel blends for distributed hydrogen generation. *Int. J. Hydrogen Energy* **2015**, *40*, 75–84. [CrossRef]
10. Pasel, J.; Samsun, R.C.; Tschauder, A.; Peters, R.; Stolten, D. A novel reactor type for autothermal reforming of diesel fuel and kerosene. *Appl. Energy* **2015**, *150*, 176–184. [CrossRef]
11. Achouri, I.E.; Abatzoglou, N.; Fauteux-Lefebvre, C.; Braidy, N. Diesel steam reforming: Comparison of two nickel aluminate catalysts prepared by wet-impregnation and co-precipitation. *Catal. Today* **2013**, *207*, 13–20. [CrossRef]
12. Xu, L.; Mi, W.; Su, Q. Hydrogen production through diesel steam reforming over rare-earth promoted Ni/γ-Al2O3 catalysts. *J. Nat. Gas Chem.* **2011**, *20*, 287–293. [CrossRef]
13. Brown, L.F. A comparative study of fuels for on-board hydrogen production for fuel-cell-powered automobiles. *Int. J. Hydrogen Energy* **2001**, *26*, 381–397. [CrossRef]

14. Tsolakis, A.; Megaritis, A.; Golunski, S.E. Reaction profiles during exhaust-assisted reforming of diesel engine fuels. *Energy Fuels* **2005**, *19*, 744–752. [CrossRef]
15. Thormann, J.; Pfeifer, P.; Schubert, K.; Kunz, U. Reforming of diesel fuel in a micro reactor for APU systems. *Chem. Eng. J.* **2008**, *135*, S74–S81. [CrossRef]
16. Ra, Y.; Reitz, R.D. A reduced chemical kinetic model for IC engine combustion simulations with primary reference fuels. *Combust. Flame* **2008**, *155*, 713–738. [CrossRef]
17. Pitz, W.J.; Mueller, C.J. Recent progress in the development of diesel surrogate fuels. *Prog. Energy Combust. Sci.* **2011**, *37*, 330–350. [CrossRef]
18. Wang, H.; Yao, M.; Yue, Z.; Jia, M.; Reitz, R.D. A reduced toluene reference fuel chemical kinetic mechanism for combustion and polycyclic-aromatic hydrocarbon predictions. *Combust. Flame* **2015**, *162*, 2390–2404. [CrossRef]
19. Ra, Y.; Reitz, R.D. A combustion model for IC engine combustion simulations with multi-component fuels. *Combust. Flame* **2011**, *158*, 69–90. [CrossRef]
20. Abashar, M. Steam reforming of *n*-heptane for production of hydrogen and syngas. *Int. J. Hydrogen Energy* **2013**, *38*, 861–869. [CrossRef]
21. Hamoule, T.; Peyrovi, M.; Rashidzadeh, M.; Toosi, M. Catalytic reforming of *n*-heptane over Pt/Al-HMS catalysts. *Catal. Commun.* **2011**, *16*, 234–239. [CrossRef]
22. González-Marcos, M.; Iñarra, B.; Guil, J.; Gutiérrez-Ortiz, M. Development of an industrial characterisation method for naphtha reforming bimetallic Pt-Sn/Al2O3 catalysts through *n*-heptane reforming test reactions. *Catal. Today* **2005**, *107*, 685–692. [CrossRef]
23. Susu, A.A. Comparative study of aromatization selectivity during N-heptane reforming on sintered Pt/Al2O3 and Pt-Re/Al2O3 catalysts. *J. Chem. Technol. Biotechnol.* **2008**, *83*, 928–942. [CrossRef]
24. Lakhapatri, S.L.; Abraham, M.A. Deactivation due to sulfur poisoning and carbon deposition on Rh-Ni/Al2O3 catalyst during steam reforming of sulfur-doped *n*-hexadecane. *Appl. Catal. A Gen.* **2009**, *364*, 113–121. [CrossRef]
25. Villoria, J.; Alvarez-Galvan, M.C.; Al-Zahrani, S.; Palmisano, P.; Specchia, S.; Specchia, V.; Fierro, J.; Navarro, R.; Al-Zahrani, S.; Yerga, R.N. Oxidative reforming of diesel fuel over LaCoO3 perovskite derived catalysts: Influence of perovskite synthesis method on catalyst properties and performance. *Appl. Catal. B Environ.* **2011**, *105*, 276–288. [CrossRef]
26. Craciun, R.; Shereck, B.; Gorte, R. Kinetic studies of methane steam reforming on ceria-supported Pd. *Catal. Lett.* **1998**, *51*, 149–153. [CrossRef]
27. Wang, X.; Gorte, R. A study of steam reforming of hydrocarbon fuels on Pd/ceria. *Appl. Catal. A Gen.* **2002**, *224*, 209–218. [CrossRef]
28. Faure, R.; Rossignol, F.; Chartier, T.; Bonhomme, C.; Maître, A.; Etchegoyen, G.; Del Gallo, P.; Gary, D. Alumina foam catalyst supports for industrial steam reforming processes. *J. Eur. Ceram. Soc.* **2011**, *31*, 303–312. [CrossRef]
29. Choi, W.Y.; Lee, J.W.; Kim, M.J.; Park, C.J.; Jeong, Y.H.; Choi, H.-Y.; Park, N.-K.; Lee, T.J. Durability tests of Rh/Al-Ce-Zr catalysts coated on NiCrAl metal foam for ATR of dodecane at high temperature. *Int. J. Precis. Eng. Manuf. Technol.* **2017**, *4*, 183–189. [CrossRef]
30. Xu, D.; Wu, B.; Ren, P.; Wang, S.; Huo, C.; Zhang, B.; Guo, W.; Huang, L.; Wen, X.; Qin, Y.; et al. Controllable deposition of Pt nanoparticles into a KL zeolite by atomic layer deposition for highly efficient reforming of *n*-heptane to aromatics. *Catal. Sci. Technol.* **2017**, *7*, 1342–1350. [CrossRef]
31. Alvarez-Galvan, M.C.; Yerga, R.N.; Rosa, F.; Briceño, Y.; Alvarez, F.G.; Fierro, J. Performance of La, Ce-modified alumina-supported Pt and Ni catalysts for the oxidative reforming of diesel hydrocarbons. *Int. J. Hydrogen Energy* **2008**, *33*, 652–663. [CrossRef]
32. Twigg, M.V. Catalytic control of emissions from cars. *Catal. Today* **2011**, *163*, 33–41. [CrossRef]
33. Zheng, T.; He, J.; Zhao, Y.; Xia, W.; He, J. Precious metal-support interaction in automotive exhaust catalysts. *J. Rare Earths* **2014**, *32*, 97–107. [CrossRef]
34. Shaula, A.; Karavai, O.; Ivanova, Y.; Mikhalev, S.; Tarelho, L. Strontium ferrite as a three-way catalyst component. *Mater. Lett.* **2018**, *216*, 273–276. [CrossRef]
35. Sugiura, M. Oxygen Storage Materials for Automotive Catalysts: Ceria-Zirconia Solid Solutions. *Catal. Surv. Asia* **2003**, *7*, 77–87. [CrossRef]

36. Karatzas, X.; Jansson, K.; Dawody, J.; Lanza, R.; Pettersson, L.J. Microemulsion and incipient wetness prepared Rh-based catalyst for diesel reforming. *Catal. Today* **2011**, *175*, 515–523. [CrossRef]
37. Han, Z.; Wang, J.; Yan, H.; Shen, M.; Wang, J.; Wang, W.; Yang, M. Performance of dynamic oxygen storage capacity, water–gas shift and steam reforming reactions over Pd-only three-way catalysts. *Catal. Today* **2010**, *158*, 481–489. [CrossRef]
38. Salazar-Villalpando, M.D. Syn-gas generation in the absence of oxygen and isotopic exchange reactions over Rh & Pt/doped-ceria catalysts. *Int. J. Hydrogen Energy* **2012**, *37*, 2121–2128.
39. Nevalainen, P.; Kinnunen, N.M.; Kirveslahti, A.; Kallinen, K.; Maunula, T.; Keenan, M.; Suvanto, M. Formation of NH 3 and N 2 O in a modern natural gas three-way catalyst designed for heavy-duty vehicles: The effects of simulated exhaust gas composition and ageing. *Appl. Catal. A Gen.* **2018**, *552*, 30–37. [CrossRef]
40. Granlund, M.Z.; Görke, O.; Pfeifer, P.; Pettersson, L.J. Comparison between a micro reactor with multiple air inlets and a monolith reactor for oxidative steam reforming of diesel. *Int. J. Hydrogen Energy* **2014**, *39*, 18037–18045. [CrossRef]
41. Mota, N.; Alvarez-Galvan, M.C.; Al-Zahrani, S.; Navarro, R.; Fierro, J.; Al-Zahrani, S. Diesel fuel reforming over catalysts derived from LaCo1−xRuxO3 perovskites with high Ru loading. *Int. J. Hydrogen Energy* **2012**, *37*, 7056–7066. [CrossRef]
42. Grote, M.; Maximini, M.; Yang, Z.; Engelhardt, P.; Köhne, H.; Lucka, K.; Brenner, M. Experimental and computational investigations of a compact steam reformer for fuel oil and diesel fuel. *J. Power Sources* **2011**, *196*, 9027–9035. [CrossRef]
43. Wang, Z.; Huang, H.; Liu, H.; Zhou, X. Self-sustained electrochemical promotion catalysts for partial oxidation reforming of heavy hydrocarbons. *Int. J. Hydrogen Energy* **2012**, *37*, 17928–17935. [CrossRef]
44. Huang, H.; Wang, Z.; Zhou, X.; Liu, H.; Wei, Y.; Pramuanjaroenkij, A.; Bordas, A.; Page, M.; Cai, S.; Zhang, X. Development and Study of Self-Sustained Electrochemical Promotion Catalysts for Hydrocarbon Reforming. *ECS Trans.* **2013**, *58*, 243–254. [CrossRef]
45. Chen, H.; Wang, X.; Pan, Z.; Xu, H. Numerical Simulation and Experimental Investigation of Diesel Fuel Reforming over a Pt/CeO2-Al2O3 Catalyst. *Energies* **2019**, *12*, 1056. [CrossRef]
46. Wang, H.; Jiao, Q.; Yao, M.; Yang, B.; Qiu, L.; Reitz, R.D. Development of an *n*-heptane/toluene/polyaromatic hydrocarbon mechanism and its application for combustion and soot prediction. *Int. J. Engine Res.* **2013**, *14*, 434–451. [CrossRef]
47. Koop, J.; Deutschmann, O. Detailed surface reaction mechanism for Pt-catalyzed abatement of automotive exhaust gases. *Appl. Catal. B Environ.* **2009**, *91*, 47–58. [CrossRef]
48. Chatterjee, D.; Deutschmann, O.; Warnatz, J. Detailed surface reaction mechanism in a three-way catalyst. *Faraday Discuss.* **2001**, *119*, 371–384. [CrossRef]
49. Chen, H.; Shen, H.; Wu, T.; Zuo, C. Numerical simulation and experimental research on combustion characteristics of compression-ignition engine under an O2/CO2 atmosphere. *HKIE Trans.* **2017**, *24*, 121–132. [CrossRef]
50. Internet: Chemkin@reactiondesign.com. Available online: http://www.reactiondesign.com/products/chemkin/chemkin-2/ (accessed on 6 March 2019).
51. Tsolakis, A.; Golunski, S. Sensitivity of process efficiency to reaction routes in exhaust-gas reforming of diesel fuel. *Chem. Eng. J.* **2006**, *117*, 131–136. [CrossRef]
52. Tsolakis, A. Catalytic exhaust gas fuel reforming for diesel engines?effects of water addition on hydrogen production and fuel conversion efficiency. *Int. J. Hydrogen Energy* **2004**, *29*, 1409–1419. [CrossRef]
53. Mariagiovanna, M. On-board fuel processor modelling for hydrogen-enriched gasoline fuelled engine. *Int. J. Hydrogen Energy* **2005**, *30*, 1483–1490.
54. Moon, D.J.; Sreekumar, K.; Lee, S.D.; Lee, B.G.; Kim, H.S. Studies on gasoline fuel processor system for fuel-cell powered vehicles application. *Appl. Catal. A Gen.* **2001**, *215*, 1–9. [CrossRef]
55. Karatzas, X.; Dawody, J.; Grant, A.; Svensson, E.E.; Pettersson, L.J. Zone-coated Rh-based monolithic catalyst for autothermal reforming of diesel. *Appl. Catal. B Environ.* **2011**, *101*, 226–238. [CrossRef]